

HDOI L

Copy 243  
RM L57J24

20 JAN 1952

~~CONFIDENTIAL~~

16214  
16484

NACA RM L57J24

TECH LIBRARY KAFB, NM  
0144738

**NACA**

# RESEARCH MEMORANDUM

7812

FREE-FLIGHT PRESSURE MEASUREMENTS OVER A FLARE-STABILIZED  
ROCKET MODEL WITH A MODIFIED VON KÁRMÁN NOSE  
FOR MACH NUMBERS UP TO 4.3

By William M. Bland, Jr., and Ronald Kolenkiewicz

Langley Aeronautical Laboratory  
Langley Field, Va.

CLASSIFIED DOCUMENT

This material contains information affecting the National Defense of the United States within the meaning of the espionage laws, Title 18, U.S.C., Secs. 793 and 794, the transmission or revelation of which in any manner to an unauthorized person is prohibited by law.

## NATIONAL ADVISORY COMMITTEE FOR AERONAUTICS

WASHINGTON  
January 13, 1958

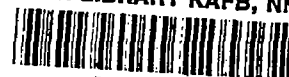
~~CONFIDENTIAL~~

CLASSIFIED (or changed to Unclassified)  
by authority of NSA Tech TB Announcement #17  
(OFFICER AUTHORIZED TO CHANGE)

By 14/1/2006  
NAME AND

NK  
GRADE OF OFFICER MAKING CHANGE)

16 Feb 61  
DATE



## NATIONAL ADVISORY COMMITTEE FOR AERONAUTICS

## RESEARCH MEMORANDUM

FREE-FLIGHT PRESSURE MEASUREMENTS OVER A FLARE-STABILIZED  
ROCKET MODEL WITH A MODIFIED VON KÁRMÁN NOSE  
FOR MACH NUMBERS UP TO 4.3

By William M. Bland, Jr., and Ronald Kolenkiewicz

## SUMMARY

Pressures were measured during a free-flight test at zero angle of attack over a rocket model consisting of a modified Von Kármán nose in combination with a cylindrical center section and a  $10^\circ$  half-angle flare. The static pressures were measured at two nose stations, one cylinder station, and two flare stations. The data were obtained at Mach numbers up to 4.3, for which the corresponding Reynolds number per foot was  $14.8 \times 10^6$  during the first- and second-stage accelerating and coasting periods of a four-stage model. The experimental pressures agreed in general with those predicted by the second-order and Taylor-Maccoll theories. The probability of separation at the cylinder-flare junction of the model is considered. The pressure distribution on the flare was found to compare well with that on the flare of a similar free-flight model previously tested.

## INTRODUCTION

In conjunction with the problem of aerodynamic heating currently being investigated by the Pilotless Aircraft Research Division of the Langley Aeronautical Laboratory, there has been a need for experimental body pressure data in order that the heat-transfer data may be correlated on the basis of measured local flow conditions. Consequently, instrumentation for pressure measurements was included in a four-stage hypersonic flare-stabilized model that was approximately a scaled version of the heat-transfer model of references 1 and 2. This model was also similar in some respects to the heat-transfer model of reference 3.

Pressure measurements made on the nose, cylinder, and flare of the model are presented in this report for Mach numbers up to 4.3. The model

attained a maximum Mach number of 8.4. However, the part of the flight test at the higher Mach numbers occurred at much higher altitudes than anticipated because the desired flight path was not adhered to. Consequently, the instrumentation installed in the model was unable to measure accurately the low pressures encountered during the high-speed portion of the flight test. The flight test was conducted at the Langley Pilotless Aircraft Research Station at Wallops Island, Va.

The pressure data are compared with some existing theoretical data for obtaining a pressure distribution over a body in supersonic flight, and the probability of separation at the cylinder-flare junction of the model is considered.

#### SYMBOLS

$C_p$	pressure coefficient, $\frac{144(p - p_\infty)}{q_\infty}$
$D$	diameter of cylinder, in.
$l_0$	length of model, measured from station zero
$M$	Mach number
$p$	static pressure, lb/sq in.
$q$	dynamic pressure, lb/sq ft
$R$	Reynolds number, $\frac{\rho V l}{\mu}$ , where $l$ is a characteristic length
$r$	radius, in.
$t$	time from start of test flight, sec
$V$	velocity, ft/sec
$x_0$	axial distance from station zero, in.
$\rho$	density of air, slugs/cu ft
$\mu$	viscosity of air, slugs/ft-sec
Subscripts:	
$\infty$	free-stream conditions

- A station on Von Kármán nose (fig. 1(b))
- B station on Von Kármán nose (fig. 1(b))
- C station on cylinder (fig. 1(b))
- D station on flare (fig. 1(b))
- E station on flare (fig. 1(b))
- c station on cylinder for model of reference 3
- 1 first station on flare for model of reference 3
- 2 second station on flare for model of reference 3
- 3 third station on flare for model of reference 3
- f denotes station at the beginning of the flare

#### MODEL DESCRIPTION

The model, which consisted of a modified Von Kármán nose shape of fineness ratio 5.0, a cylinder of fineness ratio 5.0, and a frustum of a  $10^\circ$  semivertex angle cone, is shown in a sketch in figure 1 and in a photograph in figure 2.

The model, except for the antenna and the nose tip, was in general a 1.083-scale model of the configuration tested in references 1 and 2. The antenna fins used on the model in references 1 and 2 were replaced by an antenna which was formed by separating the model nose with insulation from station 8 to 8.25 and using the forward portion of the nose as an antenna. The Von Kármán nose was modified by attaching a  $10^\circ$  semivertex angle cone at its point of tangency on the Von Kármán nose. This point of tangency occurs at station 3.679 (8.35 percent of the Von Kármán nose), the stations being measured in inches from the apex of the cone. The cone was then blunted as shown in figure 1(a). The nose of the model back to station 6.384 was machined from stainless steel, and from station 6.384 to station 11, from mild steel.

Between stations 11 and 35.75 the skin was fabricated from 1/32-inch-thick Inconel. A radiation shield was mounted under the skin to protect the instruments and telemeter enclosed in this portion of the model from heat radiated inward when the skin reached high temperatures. This radiation shield was made of 1/32-inch-thick magnesium alloy and only touched

the Inconel skin at stations 11 and 35.750. Between stations 35.750 and 37.125 was a steel structure intended to be part of an antenna that was not used. Rearward of station 37.125 the model was made of 1/64-inch-thick stainless steel with the tail flare (starting at station 66.488) being supported internally by a balsa and mahogany plywood structure. The entire external surface of the model was polished.

#### INSTRUMENTATION AND ACCURACY

Pressures at several locations on the body and accelerations along each body axis were measured with 10 instruments mounted in the body. Static pressures were measured at five stations located along the surface as shown in figure 1(b). Pressures at four stations (A, B, D, and E) were measured directly with instruments that could measure pressures to 14 lb/sq in. gage with a possible error of  $\pm 0.28$  lb/sq in. The pressure at station C was measured with reference to the pressure at station D with a differential instrument that could measure a pressure difference to 3.5 lb/sq in. with a possible error of  $\pm 0.07$  lb/sq in. The static pressure at station C was obtained from this pressure differential and the pressure at station D.

Other instrumentation consisted of ground-based radar units for measuring model velocity and for obtaining the position of the model in space. A rawinsonde carried aloft by a balloon provided measurements of atmospheric conditions at the time of the flight test.

#### TEST

The four-stage propulsion system used in this test, which was the same as that used in the investigation of reference 1, consisted of a Nike (M5 JATO) booster for the first and second stages, a T40 motor for the third stage, and a T55 motor for the fourth stage. The model, which contained the T55 motor, and the three booster stages are shown in figure 3 as they appeared on the launcher. All data presented were obtained before third-stage ignition. The trajectory made by the model while the data were being obtained is shown in figure 4. Time histories of atmospheric pressure, density, dynamic pressure, and altitude are shown in figure 5. The time histories of Mach number, velocity, and Reynolds number per foot are shown in figure 6.

The velocity during this test was obtained for the time interval up to 22.5 seconds by Doppler radar, for the interval from 22.5 to 25 seconds by integrating the accelerometer data, and for time after

25 seconds by differentiating the range data as obtained from ground-based radar measurements.

## RESULTS AND DISCUSSION

The trajectory and the time histories of the flight conditions shown in figures 4, 5, and 6 were nearly the same as those of the model in references 1 and 2. Similar aerodynamic heating conditions should therefore exist on the two models. The model of references 1 and 2 at a station of 83.8 percent of its Von Kármán nose had a maximum measured skin temperature of  $1,155^{\circ}$  R ( $t = 23$  sec) during the similar flight period.

Time histories of pressure obtained during this test are shown in figure 7. Because of the uncertainty of the pressure data at low magnitudes resulting from the fixed possible instrument errors, pressure-dependent parameters were computed only for times prior to 22 seconds. Also because of the scatter in the measurements, probably caused by unsteady local flow conditions, these parameters were not presented for Mach numbers less than 1.5. Absence of static pressure data during certain times at station C is due to the fact that these values were measured differentially between stations C and D (fig. 8) and during several intervals this instrument went off scale. The time history of the difference between the static pressure on the flare, station D, and on the cylinder ahead of the flare, station C, is shown in figure 8. The tendency of this curve to approach zero between  $t = 10$  seconds and  $t = 15$  seconds and after  $t = 20$  seconds may mostly be accounted for by a decreasing Mach number in these ranges.

Figure 9 shows both experimental and theoretical (refs. 4 and 5) variations of pressure coefficient with free-stream Mach number at all static pressure orifice stations. More than one experimental point for a given orifice at a Mach number was obtained when the model went through the same Mach number more than once (before a time of 22 seconds). When this occurred these points agreed well.

In figure 9(a) the experimental points on the nose, stations A and B, are compared with theoretical values from reference 4 which were calculated for a Von Kármán nose with a short conical tip. The experimental points for orifice A, located at 10.33 percent of the Von Kármán nose length, were somewhat above the second-order theoretical values (ref. 4) below Mach number 3, but agreed well at the higher Mach numbers. Experimental points for orifice B, located at 27.33 percent of the Von Kármán nose length, were considerably above values predicted by the second-order theory for a Von Kármán nose (ref. 4) in the low Mach number region and agreed better as the Mach number increased. It should be noted that large differences between the experimental and theoretical

pressure coefficients are not accompanied by correspondingly large differences in the pressures used to derive these coefficients. Some results for orifice B, shown in table I, illustrate this fact. From this comparison it can be seen that pressures estimated with theoretical pressure coefficients that do not correlate well with experiment may not be much in error.

Further disagreement between experiment and theory for orifices A and B may be attributed to the fact that the theoretical values from reference 4 were necessarily obtained (for computational reasons) for a nose with a sharp cone tangent to the Von Kármán nose at a station that was less than 5 percent of the nose length. The experimental data of the present test were obtained from a Von Kármán nose having a blunted cone tangent to the Von Kármán nose at 8.35 percent of nose length.

The experimental values of the pressure coefficient at station C, located on the cylinder, are shown in figure 9(b). In the region where the values of the pressure coefficients were not obtained, an upper limit or boundary may be drawn. This upper limit may be calculated by observing that the differential pressure,  $p_D - p_C$ , went off the high side of its scale; that is,  $p_D - p_C \geq 3.5$  lb/sq in. Since the experimental static pressure  $p_D$  is a known quantity, the inequality may be solved for  $p_C$  and an upper limit for experimental pressure coefficients at station C may be obtained and drawn in as shown in figure 9(b).

Pressure coefficients at stations D and E, located on the flare, are compared in figure 9(b) with Taylor-Maccoll wedge and cone theory (ref. 5). For an unseparated flow it would be expected that the experimental points for these two stations would lie between values obtained by wedge and cone theory, with the forward orifice (station D) nearer the values given by wedge theory and the rear orifice (station E) nearer that given by cone theory. This may be seen to hold true up to a Mach number of about 2.3, after which the pressure coefficient values of orifice D cross over and drop below those of orifice E. At a Mach number of about 3.25 the pressure coefficients at orifice D drop below the region between wedge and cone theory and continue to decrease as the Mach number increases. Taking instrument accuracy into account would not raise the experimental points at D enough to remain between the two theoretical curves. The foregoing results may be due to separation of the boundary layer at the cylinder-flare junction. The differential pressure between orifices C and D, presented in figure 8, was measured in order to determine if the flow had separated ahead of the flare. For a supersonic flow that does not separate, a shock wave would form at the beginning of the flare between stations C and D. This shock wave would cause a higher static pressure at D than at C, the difference being positive if taken in the same sense as figure 8. As separation occurs the shock wave would

move forward until, when it moves forward of station C, the static pressure differential,  $P_D - P_C$ , would be zero.

In figure 8, except for time near take-off, the value of  $P_D - P_C$  is zero only after  $t = 35$  seconds. This result is attributed to increasing altitude and decreasing Mach number rather than to separated flow. In this test the differential pressure measurements across the flare-cylinder junction of the model,  $P_D - P_C$ , do not indicate separated flow; however, the distance between orifice C and the beginning of the flare is 3.020 inches. A separated flow in this region which had not extended forward to orifice C would not be indicated by the differential pressure,  $P_D - P_C$ .

The relative change in magnitude of the pressure coefficients at the forward and rearward flare stations, as previously noted, also occurred on the model of reference 3 which consisted of a  $25^\circ$  total angle conical nose, a cylinder of fineness ratio 4.8, and a frustum of a  $10^\circ$  semivertex angle cone. A portion of the data from reference 3 is presented in figure 10 along with data from this test. Figure 10 shows a distribution of pressure coefficients along the body at various Mach numbers. The model of reference 3 was superimposed upon the model of the present investigation in such manner as to make the station at the beginning of their flares coincide. The experimental and theoretical (ref. 4) pressure-coefficient distributions are shown over a portion of the nose of the body. The pressure coefficient on the cylinder for the model of reference 3 may be seen to be about zero.

The flares of both models, shown in figure 10, had  $10^\circ$  semivertex angles. For the model of reference 3 the pressure coefficients at the first flare station,  $C_{p,1}$ , were greater than those of the second flare station,  $C_{p,2}$ , for Mach numbers less than 2. For Mach numbers above 2.5 the relative position of these points changed. Similar behavior was observed in the same Mach number range for corresponding flare stations,  $C_{p,D}$  and  $C_{p,E}$  for the model of this test. A third flare pressure coefficient,  $C_{p,3}$ , measured farther to the rear on the model of reference 3 and pressure coefficients predicted by wedge and cone theories (ref. 5) are also shown in figure 10. Table II gives the value of the Reynolds number for the two models compared in figure 10.

Results of a wind-tunnel test of a scale model of the vehicle used in the present investigation are presented in reference 6. These results indicate that at Mach number 6.8 separation, if present, was not discernible at the cylinder-flare junction if the Reynolds number, based on cylinder diameter, exceeded  $0.6 \times 10^6$  and the flow was turbulent. The

lowest Reynolds number, based on cylinder diameter, reached by the free-flight model after launching (and before  $t = 22$  sec) was  $2.06 \times 10^6$  at Mach number 0.862. This Reynolds number is 3.44 times higher than the Reynolds number at which separation in the flare region was discernible. The results of reference 6, with differences in Mach number ignored, would substantiate doubt of significant separation at the beginning of the flare for this model.

#### CONCLUDING REMARKS

Pressures have been measured at five stations along a modified Von Kármán nose-cylinder-flare configuration in free flight at zero angle of attack to Mach number 4.3. Experimental pressure coefficients at two stations on the nose were found to be in agreement with second-order theory for Mach number greater than 2.5. Pressure measured at two succeeding flare stations indicated that the forward station had a higher static pressure than the rearward station for a Mach number below about 2.3. At higher Mach numbers the rearward station had the higher static pressure value. Separation in front of the flare could be the cause of this reversal in the relative value of the static pressures measured at the two flare stations. However, differential pressure measured across the station where the flare begins gave no indication of separation. A possible explanation is that a separated flow could have occurred between the differential pressure orifices and was therefore not indicated by the differential pressure measurements. The pressure distribution on the flare was found to compare well with that obtained for a similar free-flight model.

Langley Aeronautical Laboratory,  
National Advisory Committee for Aeronautics,  
Langley Field, Va., September 27, 1957.

## REFERENCES

1. Piland, Robert O.: Performance Measurements From a Rocket-Powered Exploratory Research Missile Flown to a Mach Number of 10.4. NACA RM L54L29a, 1955.
2. Bland, William M., Jr., and Collie, Katherine A.: Free-Flight Aerodynamic-Heating Data to Mach Number 10.4 for a Modified Von Kármán Nose Shape. NACA RM L56D25, 1956.
3. Bond, Aleck C., and Rumsey, Charles B.: Free-Flight Skin Temperature and Pressure Measurements on a Slightly Blunted  $25^\circ$  Cone-Cylinder-Flare Configuration to a Mach Number of 9.89. NACA RM L57B18, 1957.
4. Jorgensen, Leland H.: Correlation by the Hypersonic Similarity Rule of Pressure Distributions and Wave Drags for Minimum-Drag Nose Shapes at Zero Angle of Attack. NACA RM A53F12, 1953.
5. Ames Research Staff: Equations, Tables, and Charts for Compressible Flow. NACA Rep. 1135, 1953. (Supersedes NACA TN 1428.)
6. Becker, John V., and Korycinski, Peter F.: Heat Transfer and Pressure Distribution at a Mach Number of 6.8 on Bodies With Conical Flares and Extensive Flow Separation. NACA RM L56F22, 1956.

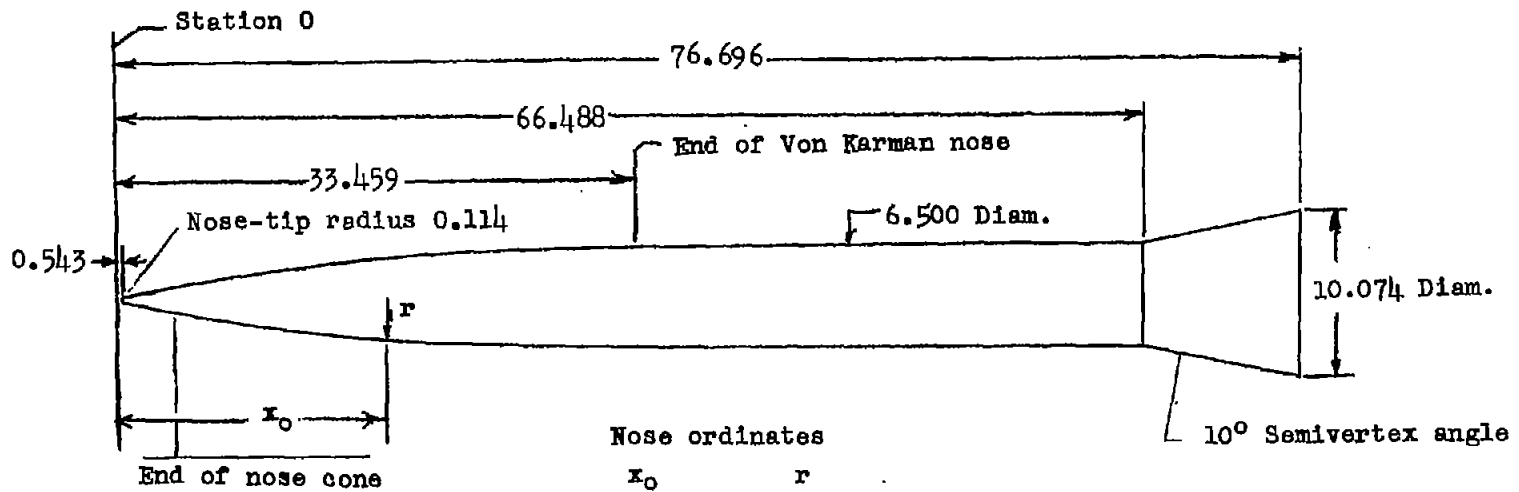
TABLE I.- TYPICAL VALUES FOR ORIFICE B<sup>1</sup>

$M_\infty$	Percentage difference in static pressure	Approximate portion due to instrument inaccuracy	Percentage difference in pressure coefficient	Approximate portion due to instrument inaccuracy
2.5	8.0	±3.0	45.7	±30
3.0	5.5	±3.0	27.3	±15
3.75	7.4	±3.0	23.2	±10

<sup>1</sup>At a free-stream Mach number of 2.5 the percentage difference between the measured static pressure and theoretical static pressure (ref. 4) is 8.0 percent. Of this 8.0-percent difference approximately ±3.0 percent may be due to inaccuracy of the instrument. The percentage difference in the corresponding pressure coefficient is 45.7. Of this 45.7 percent, ±30 percent may be due to instrument inaccuracy.

TABLE II.- REYNOLDS NUMBERS

$M_\infty$	Present test		Reference 3	
	R/ft	$R_F$	R/ft	$R_F$
2.0	$8.13 \times 10^6$	$45.0 \times 10^6$	$5.57 \times 10^6$	$27.9 \times 10^6$
2.5	10.36	57.4	6.79	34.0
3.0	11.58	64.2	7.89	39.5
3.5	13.39	74.2	8.73	43.7
4.3	14.58	80.8	-----	-----



Nose ordinates	
$x_0$	$r$
0	0
3.679	0.648
4.219	.741
5.301	.915
6.384	1.075
7.467	1.224
8.000	1.297
8.550	1.368
9.633	1.503
10.716	1.632
11.000	1.665
13.965	1.986
17.214	2.297
20.468	2.571
23.712	2.809
26.981	3.008
30.210	3.164
33.459	3.249

(a) Sketch of model. All linear dimensions in inches.

Figure 1.- General arrangement of model.





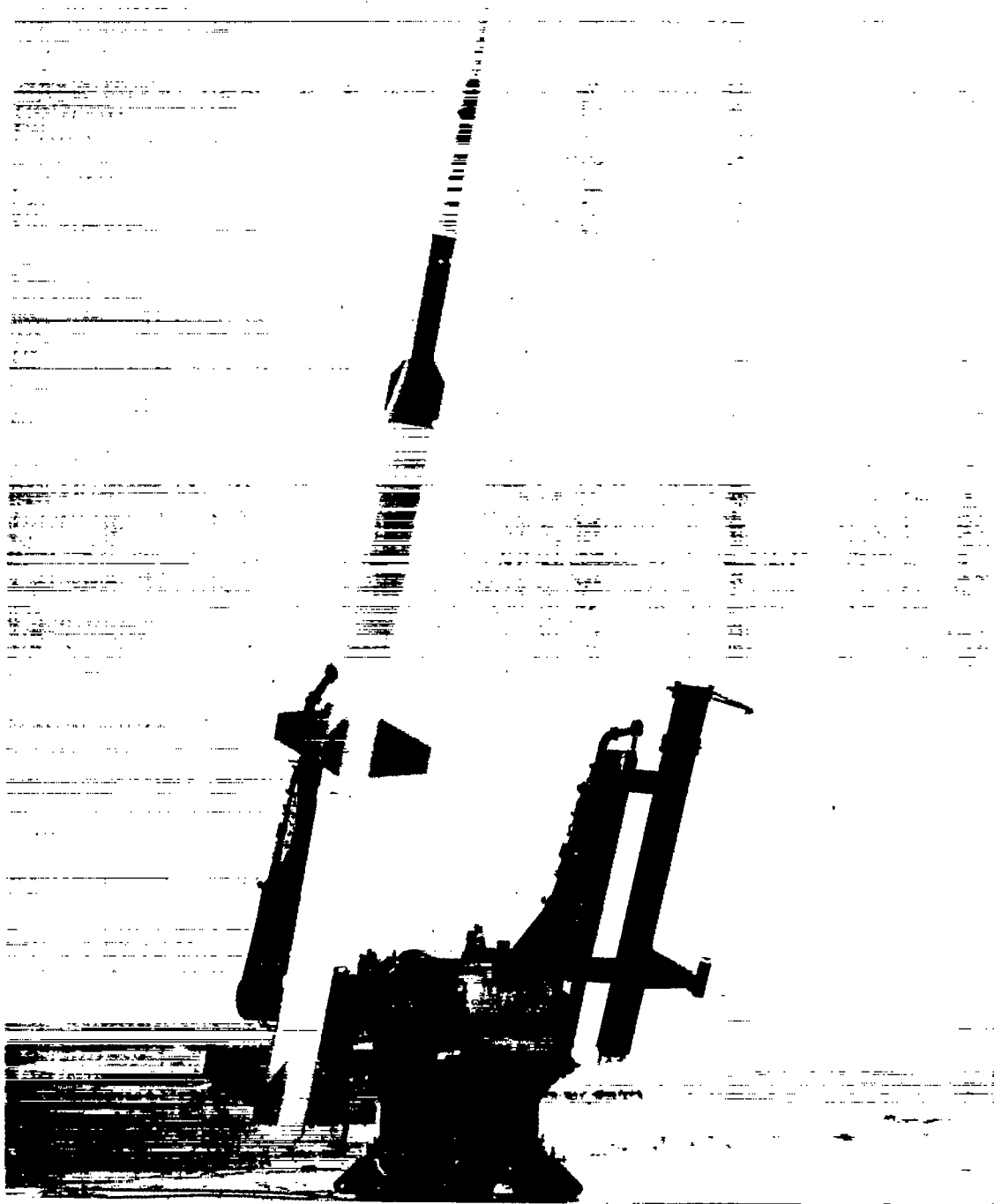


Figure 3.- Model and booster stages on launcher. L-94558

~~CONFIDENTIAL~~

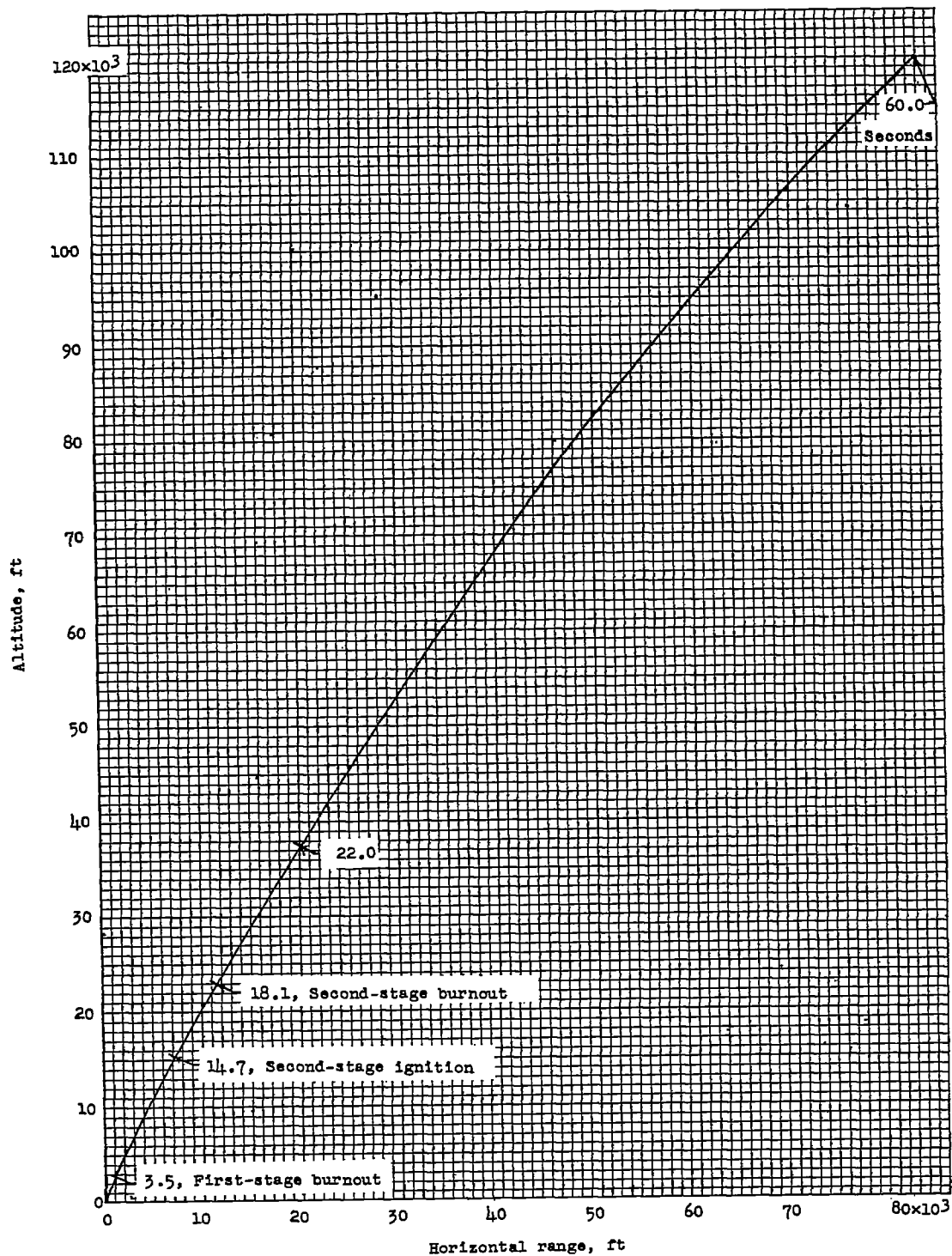


Figure 4.- A part of trajectory followed by model.

~~CONFIDENTIAL~~

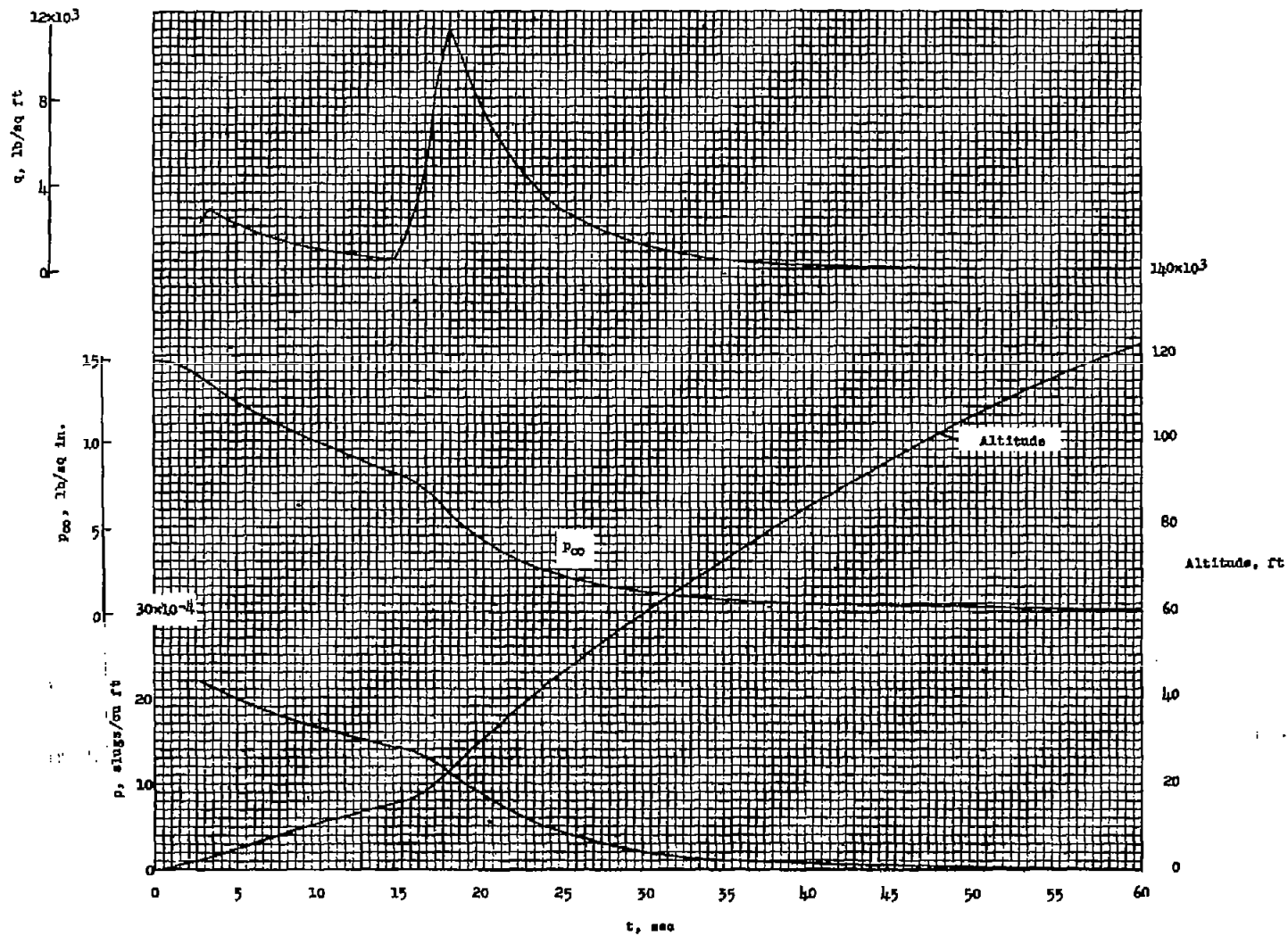


Figure 5.- Time history of dynamic pressure, ambient pressure, ambient density, and altitude of the model to 60 seconds.

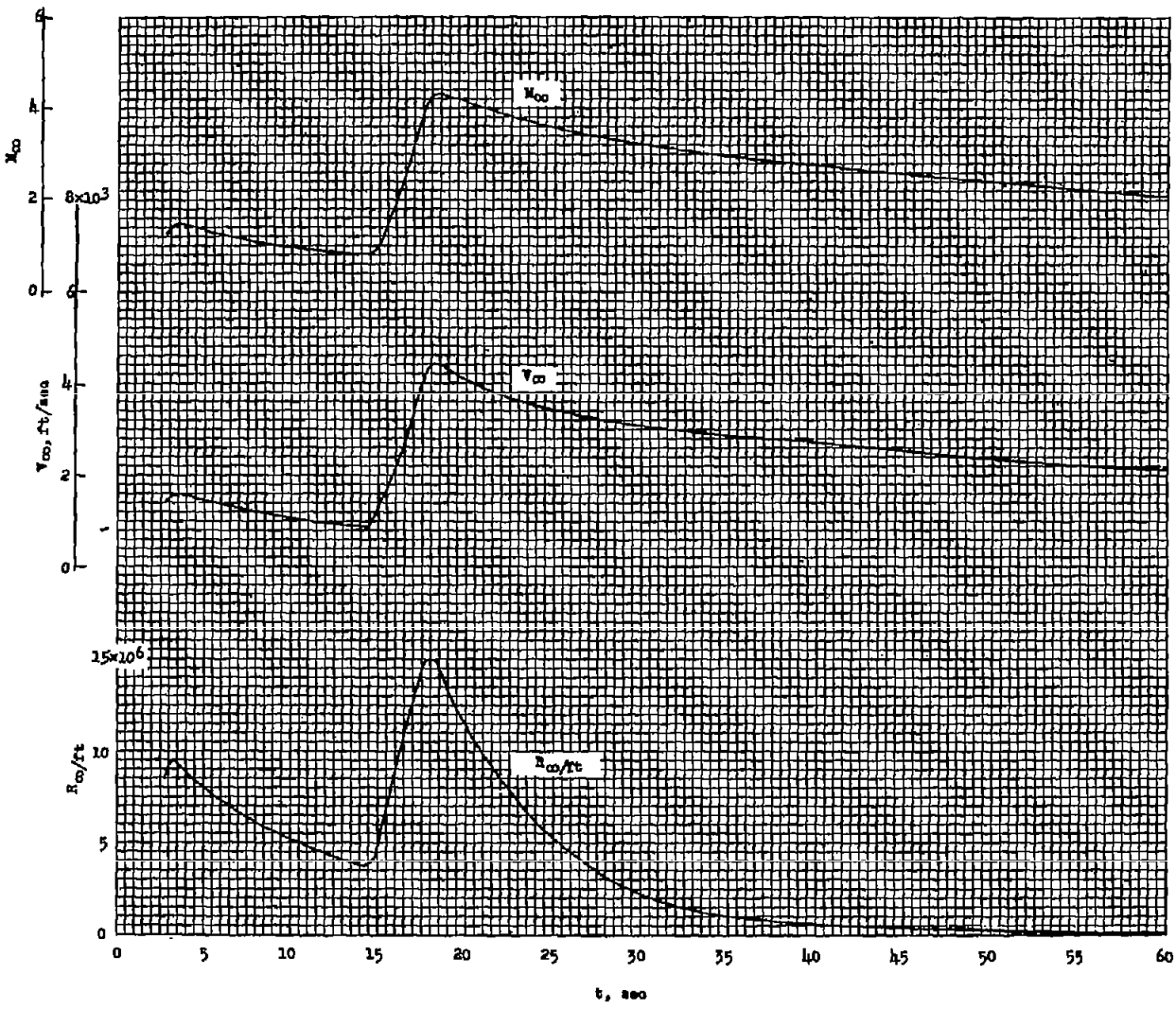


Figure 6.- Time history of Mach number, velocity, and Reynolds number per foot of the model to 60 seconds.

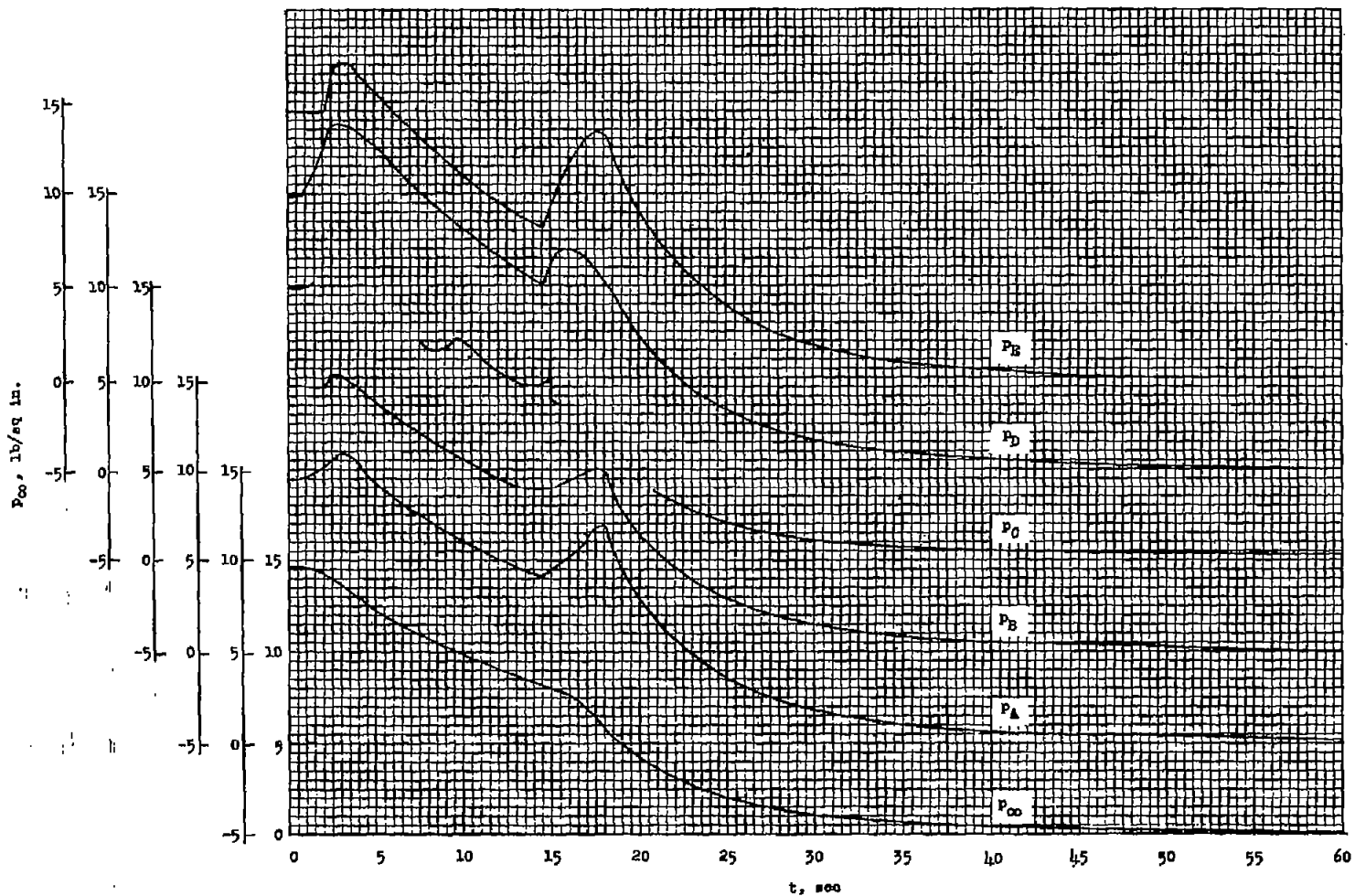


Figure 7.- Time history of the measured surface static pressures and ambient pressure.

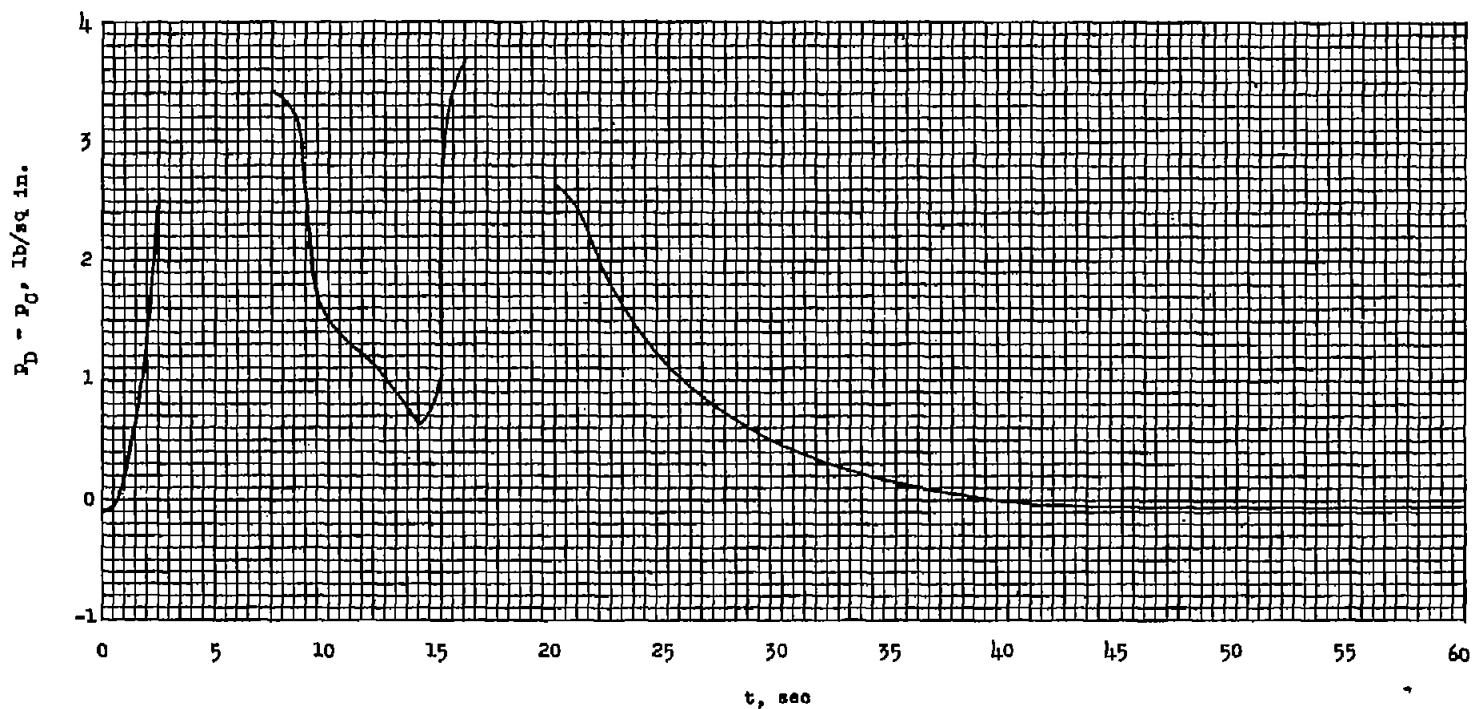
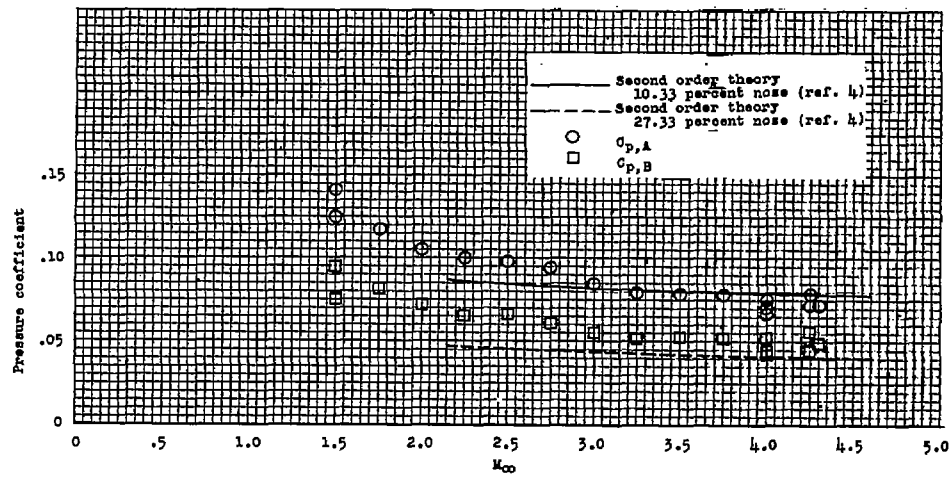
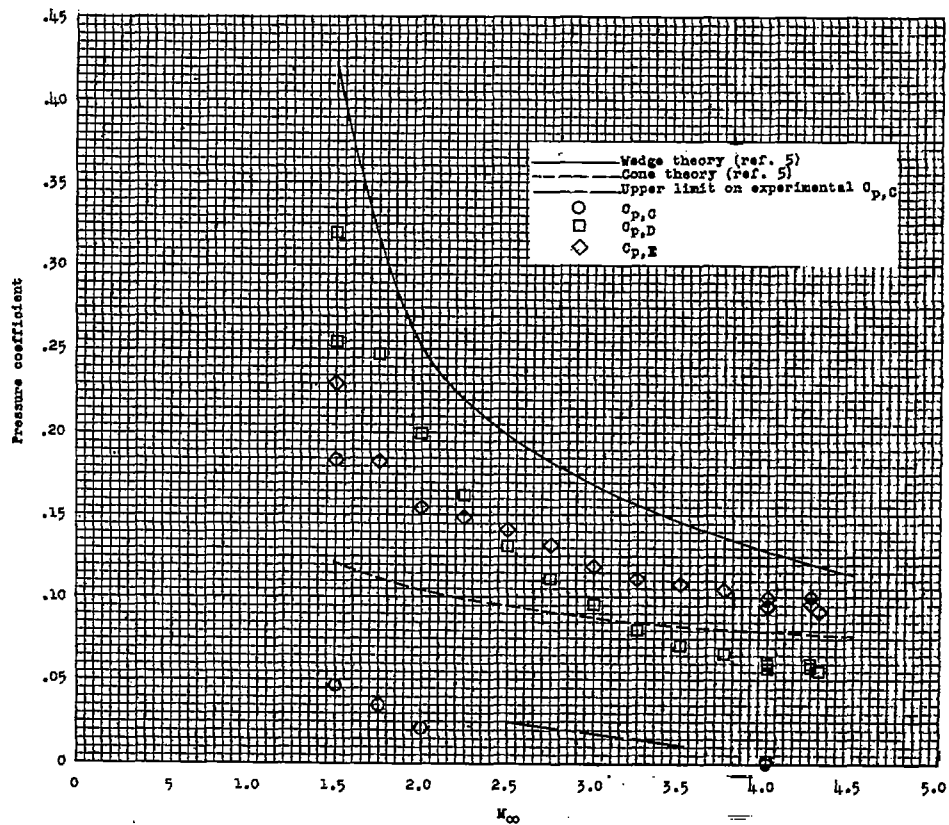


Figure 8.- Time history of the difference between the static pressure on the flare and on the cylinder ahead of the flare.



(a) Nose stations.



(b) Cylinder and flare stations C and D.

Figure 9.- Variation of the pressure coefficient with free-stream Mach number.

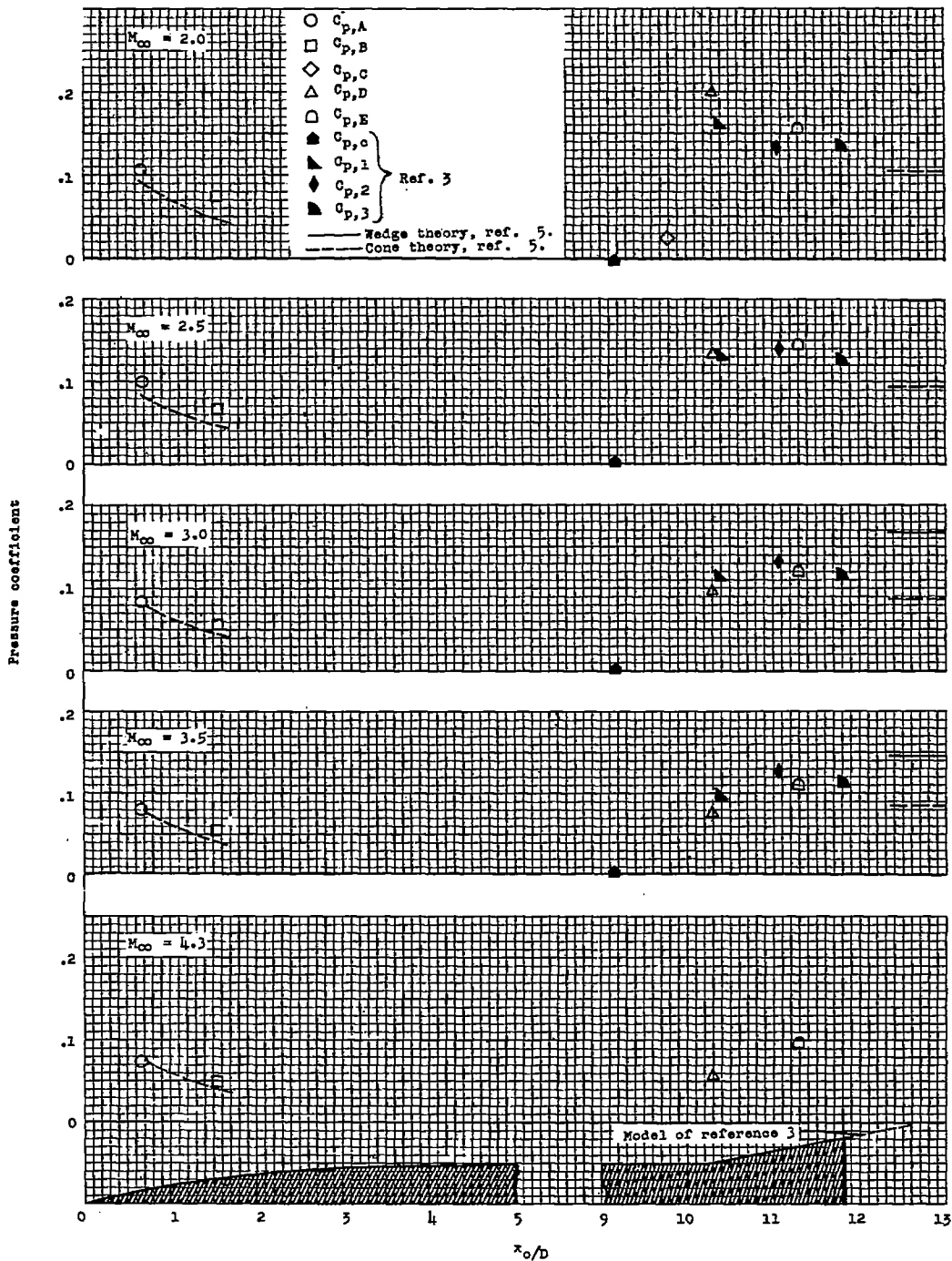


Figure 10.- Comparison of pressure coefficients obtained from present test with those from test of reference 3.

~~CONFIDENTIAL~~